Transgene distribution and immune response after ultrasound delivery of rAAV9 and PHP.B to the brain in a mouse model of amyloidosis

Rikke Hahn Kofoed,[1,2] Stefan Heinen,[1,2] Joseph Silburt,[1,2] Sonam Dubey,[1,2] Chinaza Lilian Dibia,[1,2] Miriam Maes,[1,2] Elizabeth M. Simpson,[3] Kullervo Hynynen,[4,5] and Isabelle Aubert[1,2]

[1]Biological Sciences, Hurvitz Brain Sciences Research Program, Sunnybrook Research Institute, Sunnybrook Health Sciences Centre, Toronto, ON M4N 3M5, Canada; [2]Department of Laboratory Medicine and Pathobiology, Temerty Faculty of Medicine, University of Toronto, Toronto, ON M5S 1A8, Canada; [3]Centre for Molecular Medicine and Therapeutics at British Columbia Children's Hospital, Department of Medical Genetics, The University of British Columbia, Vancouver, BC V5Z 4H4, Canada; [4]Physical Sciences, Sunnybrook Research Institute, Sunnybrook Health Sciences Centre, Toronto, ON M4N 3M5, Canada; [5]Department of Medical Biophysics, Temerty Faculty of Medicine, University of Toronto, Toronto, ON M5G 1L7, Canada

Efficient disease-modifying treatments for Alzheimer disease, the most common form of dementia, have yet to be established. Gene therapy has the potential to provide the long-term production of therapeutic in the brain following a single administration. However, the blood-brain barrier poses a challenge for gene delivery to the adult brain. We investigated the transduction efficiency and immunological response following non-invasive gene-delivery strategies to the brain of a mouse model of amyloidosis. Two emerging technologies enabling gene delivery across the blood-brain barrier were used to establish the minimal vector dosage required to reach the brain: (1) focused ultrasound combined with intravenous microbubbles, which increases the permeability of the blood-brain barrier at targeted sites and (2) the recombinant adeno-associated virus (rAAV)-based capsid named rAAV-PHP.B. We found that equal intravenous dosages of rAAV9 combined with focused ultrasound, or rAAV-PHP.B, were required for brain gene delivery. In contrast to rAAV9, focused ultrasound did not decrease the rAAV-PHP.B dosage required to transduce brain cells in a mouse model of amyloidosis. The non-invasive rAAV delivery to the brain using rAAV-PHP.B or rAAV9 with focused ultrasound triggered an immune reaction including major histocompatibility complex class II expression, complement system and microglial activation, and T cell infiltration.

INTRODUCTION

Alzheimer disease (AD) is the most common cause of dementia, and no disease-modifying treatments exist. Gene therapy using recombinant adeno-associated virus (rAAV) as vehicle can provide a long-term treatment after a single administration, and it has been evaluated in several clinical trials for the treatment of neurodegenerative disorders, including AD. The first rAAV-based gene therapy for AD aimed to deliver a gene-encoding nerve growth factor (NGF) through intracranial injection to rescue and stimulate cholinergic neurons.[1–3] Post-mortem analysis demonstrated that the delivery of NGF was suboptimal due to limited spread of rAAV from the site of entry and inaccurate stereotactic injection.[4] A clinical trial, currently ongoing, focuses on AD patients homozygous for apolipoprotein E4 (APOE4). Using intracisternal injections of rAAV, the goal is to deliver the protective APOE2 allele and hereby mitigate the deleterious effects of APOE4.[5] Intracisternal injection may provide a broader gene delivery to the brain compared to intraparenchymal injections used for rAAV-NGF delivery; however, it is still an invasive surgical method targeting structures in proximity to the brainstem, a vital area. Only one clinical trial, currently ongoing, is exploring a non-invasive systemic delivery method of a rAAV-encoding human telomerase reverse transcriptase (hTERT), with one arm of the study including patients receiving rAAV intrathecal administration (ClinicalTrials.gov: NCT04133454). In adults, the blood-brain barrier (BBB) poses a major challenge for the delivery of systemic rAAVs to the brain, and it remains to be determined whether the delivery method used in the rAAV-hTERT trial will provide sufficient transgene expression in brain areas where the therapeutics are most needed for efficacy. High doses of intravenous (i.v.) rAAVs can cross the BBB but also result in an unwanted immune response.[6,7] New strategies must be developed for efficient non-invasive delivery of rAAVs to the brain to overcome the limitations associated with intracranial injections and simultaneously minimize the amount of vector required when using systemic administrations.

Table 1. Information on all mice used in the study

Mouse #	Mouse strain	Sex	Age at injection	rAAV	MRIgFUS
M1-nTg	nTgCRND8	male	13 weeks	1E11 GC rAAV9	yes
F2-Tg	TgCRND8	female	12 weeks	1E11 GC rAAV9	yes
M3-Tg	TgCRND8	male	13 weeks	1E11 GC rAAV9	yes
M4-Tg	TgCRND8	male	13 weeks	1E11 GC rAAV9	yes
F5-nTg	nTgCRND8	female	12 weeks	1E11 GC rAAV9	yes
M6-nTg	nTgCRND8	male	12 weeks	1E10 GC PHP.B	yes
M7-Tg	TgCRND8	male	12 weeks	1E10 GC PHP.B	yes
M8-Tg	TgCRND8	male	11 weeks	1E10 GC PHP.B	yes
F9-nTg	nTgCRND8	female	12 weeks	1E10 GC PHP.B	yes
M10-nTg	nTgCRND8	male	12 weeks	1E10 GC PHP.B	yes
M11-nTg	nTgCRND8	male	11 weeks	1E11 GC PHP.B	yes
F12-Tg	TgCRND8	female	12 weeks	1E11 GC PHP.B	yes
M13-Tg	TgCRND8	male	11 weeks	1E11 GC PHP.B	yes
F14-nTg	nTgCRND8	female	11 weeks	1E11 GC PHP.B	yes
M15-nTg	nTgCRND8	male	11 weeks	1E11 GC PHP.B	yes
1−3	BALB/c	male	12 weeks	1E11 GC rAAV9	yes
4−6	BALB/c	female	13 weeks	1E11 GC rAAV9	yes
7−9	BALB/c	male	12 weeks	1E11 GC PHP.B	yes
10−12	BALB/c	female	13 weeks	1E11 GC PHP.B	yes

During the last 9 years, two new technologies have emerged to address the problem of effective gene delivery to the brain: (1) MRI-guided focused ultrasound[8] and (2) a new generation of rAAVs, including rAAV-PHP.B (PHP.B), which was generated through the targeted evolution of rAAV9.[9] MRI-guided focused ultrasound combined with i.v.-injected microbubbles (the combination henceforth referred to as MRIgFUS) allows a temporary increase in the permeability of the BBB in preclinical animal models and in human clinical trials.[10,11] MRIgFUS can deliver rAAVs to targeted sites in the rodent brain and spinal cord and decrease the dose needed for rAAV9 to enter the adult brain by 50-fold.[8,12–15] Furthermore, MRIgFUS can facilitate the entry of rAAV serotypes incapable of crossing the intact BBB.[12,14,15] The PHP.B vector was developed by randomly inserting 7-mer amino acids at position 588 in the rAAV9 capsid and selecting for capsids capable of transducing the brain in C57BL/6 mice.[9] This process rendered the PHP.B superior to rAAV9 in its ability to cross the BBB in susceptible Ly6A receptor-expressing animals.[16–20] However, it restricts the use of i.v. delivery to the brain using PHP.B to species with high BBB expression of certain Ly6A variants, excluding the vector's use in primates and some inbred mouse strains (e.g., BALB/c mice).[19,20] Following the invention of PHP.B, it has been envisioned to develop= a next generation of rAAVs capable of entering the human central nervous system (CNS).[17] Prior to targeting the human CNS with PHP.B for gene therapy, preclinical testing in animal models of AD is warranted to determine how the transduction efficiency and safety of the vec-

tors may be altered by the cerebrovascular pathology and chronic inflammatory state associated with AD pathology.[21,22]

This study aimed to: (1) determine the ability of PHP.B compared to rAAV9 to transduce brain cells in a transgenic animal model of amyloidosis (TgCRND8; Tg),[23] (2) investigate the potential of MRIgFUS to enhance the ability of PHP.B to transduce the brain of Tg mice and hereby decrease the amount of PHP.B needed to deliver transgenes to the brain, (3) investigate the immune response triggered by relatively low doses of i.v. rAAVs delivered non-invasively to the brain using MRIgFUS and the PHP.B capsid, and (4) determine the ability of MRIgFUS to mediate the delivery of i.v. PHP.B to the brain of animals expressing reduced levels of the V106A Ly6A variant, with low affinity to PHP.B (BALB/c mice).[17]

RESULTS

Based on the premise that anti-amyloid-β (Aβ) therapies can be of greater benefits when administered early in the course of AD progression,[24] we used 3-month-old Tg mice to investigate gene delivery. At 3 months of age, Tg mice have early signs of AD-related pathologies, making this disease stage relevant for investigation of future therapeutics.[23] Tg mice and non-Tg (nTg) littermates were randomly divided into three groups of 5 mice per group, with 2 to 3 males and females in each group. Details on individual mice and treatments are reported in Table 1.

MRIgFUS increases the delivery of rAAV9, but not PHP.B, to targeted sites in the brain

We first investigated whether MRIgFUS can reduce the i.v. PHP.B vector dose needed to transduce brain cells. Tg mice were injected i.v. with 1×10^{11} (1E11) genome copy (GC) PHP.B, a dose known to result in brain cell transduction,[9] and a 10-times lower dose of 1E10 GC PHP.B. Two spots in the cortex and striatum and two spots in the thalamus were targeted by MRIgFUS (Figure 1A) using T2-weighed (T2w) MR images (Figure 1B). Mice injected with 1E11 GC rAAV9 served as control since MRIgFUS previously has been shown to increase the brain bioavailability of this vector when injected i.v. at doses too low to cross the BBB.[8] All vectors contained the emerald green fluorescent protein (EmGFP) transgene under the control of the ubiquitous small chicken beta-actin promoter/cytomegalovirus enhancer (smCBA).[25] Relative to the contralateral side, increased BBB permeability in MRIgFUS-targeted spots was confirmed using gadodiamide (Gad) contrast and MRI (Figure 1C). No significant difference in BBB permeability was seen between mice injected with 1E11 GC rAAV9 and 1E11 GC PHP.B, or between mice injected with 1E10 GC PHP.B and 1E11 GC PHP.B (Figure 1D). There was a significantly higher BBB permeability measured in mice injected with 1E11 GC rAAV9 compared to 1E10 GC PHP.B (Figure 1D). Previous studies have demonstrated that no differences in BBB permeability following MRIgFUS treatment are seen between Tg and nTg mice in Tg mice.[26,27] MR images used for quantification of BBB permeability are all included in Figure 2. Gad enhancement is influenced by the amount of Gad injected and the variability inherent
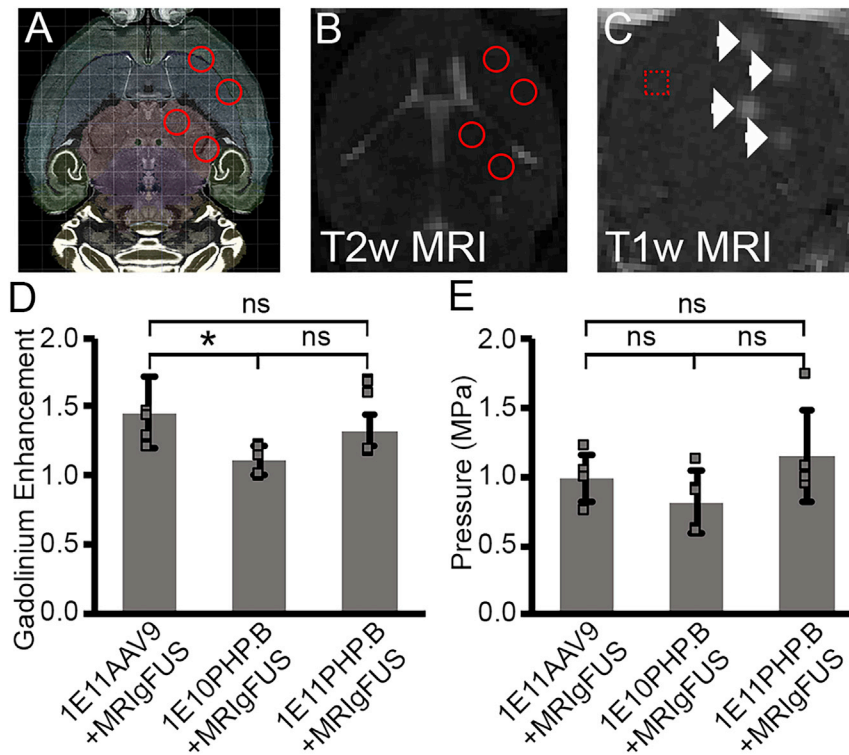
Figure 1. Gad enhancement in MRIgFUS-targeted spots

Non-transgenic (nTg) and TgCRND8 (Tg) mice were injected intravenously (i.v.) with viral vectors and treated with MRIgFUS. MRIgFUS was targeting to two spots in the cortex and striatum and two spots in the thalamus (red circles, Allen Brain Atlas; A), using T2w MRI (red circles; B). Blood-brain barrier (BBB) permeability was estimated by the detection of the MRI contrast agent Gad entering the brain in the MRIgFUS-targeted spots (white arrows) relative to the contralateral hemisphere (red square) visualized as white on T1w MR images (C). BBB permeability (D) and applied ultrasound pressure (E) were compared between mice injected with 1E11 GC rAAV9 (1E11AAV9; n = 3 Tg and 2 nTg), 1E10 GC PHP.B (1E10PHP.B; n = 2 Tg and 3 nTg), and 1E11 GC PHP.B (1E11PHP.B; n = 2 Tg and 3 nTg). Statistical comparisons were performed using one-way ANOVA and Sidak's post hoc test for multiple comparisons (D and E). Bars represent mean ± standard deviation, *$p < 0.05$, ns, not significant.

to MRIgFUS-induced BBB permeability. A measure of successful microbubble cavitation and equal application of ultrasound parameters across mice is the level of the ultrasound pressure required to reach microbubble cavitation, as detected by the hydrophone, which here was set to trigger a 50% drop in pressure. When comparing the applied ultrasound pressure, no significant differences were seen between mice injected with 1E11 GC rAAV9, 1E10 GC PHP.B, and 1E11 GC PHP.B (Figure 1E), suggesting that ultrasound parameters and microbubble cavitation produced similar effects across groups.

To evaluate transgene expression in transduced cells of the brain, Tg mice were sacrificed 3 weeks after MRIgFUS delivery, and brain sections were cut and immunostained for GFP (Figure 2; green). 4',6-diamidino-2-phenylindole (DAPI) was used as an anatomical marker (Figure 2; teal). As previously reported,[8] MRIgFUS treatment led to increased entry of i.v. rAAV9 in targeted spots, visualized by an increased GFP expression (green) at sites corresponding to Gad entry (white) (Figures 2A–2E). 1E10 GC of PHP.B in conjunction with MRIgFUS did not result in cell transduction in the MRIgFUS-targeted spots, despite confirmed BBB permeability by Gad entry (Figures 2F–2J). The injection of 1E11 GC PHP.B resulted in a widespread transduction of the brain, although with variable transduction efficiency in different areas (for instance a highly transduced spot in the thalamus can be seen in Figure 2O); however, there was no clear increase in GFP expression in MRIgFUS-targeted spots where BBB permeability was confirmed (Figures 2K–2O). These results suggest that a critical i.v. concentration of PHP.B is required to successfully cross the BBB and transduce cells in the

brain parenchyma and that, at the doses tested, MRIgFUS does not enhance the delivery of PHP.B to the brain. MRIgFUS did not deliver PHP.B to targeted areas of the brain, and it did not lower the dose of PHP.B required i.v. to transduce brain cells in C57BL/6-derived animals known to express relatively high levels of the Ly6A receptor.

Brain sections immunostained with the neuronal marker, neuronal nuclear protein (NeuN); the astrocytic marker, glial fibrillary acidic protein (GFAP); and the microglial marker, ionized calcium-binding adaptor molecule 1 (IBA1), confirmed that rAAV9 (Figure 3A) and PHP.B (Figure 3B) transduce neurons and astrocytes, but not microglia.[8,9]

Microglial activation following MRIgFUS PHP.B delivery to the brain

Intracranial injections of rAAVs in animal models can induce an immune response, characterized by an increase in microglial and complement system activation, major histocompatibility complex class II (MHC class II) expression, and T cell infiltration.[28–33] As hallmarks of activated microglia, we investigated potential increases in IBA1 expression and changes in morphology. Increased IBA1 intensity and changes in morphology were seen in MRIgFUS spots in mice injected with rAAV9 (Figures 4A–4E) but not in mice injected with 1E10 GC PHP.B and treated with MRIgFUS (Figures 4F–4J). In Tg mice injected with 1E11 GC PHP.B and treated with MRIgFUS, widespread increases in IBA1 intensity were seen, irrespective of the location of the MRIgFUS spots (Figures 4K–4O). To further quantify the activation of microglia, we used a recently developed machine learning method (morphological identification of outlier clusters, MORPHIOUS; manuscript deposited in bioRxiv).[34] The contralateral hemisphere, not treated with MRIgFUS, from mice injected with rAAV9 was used to
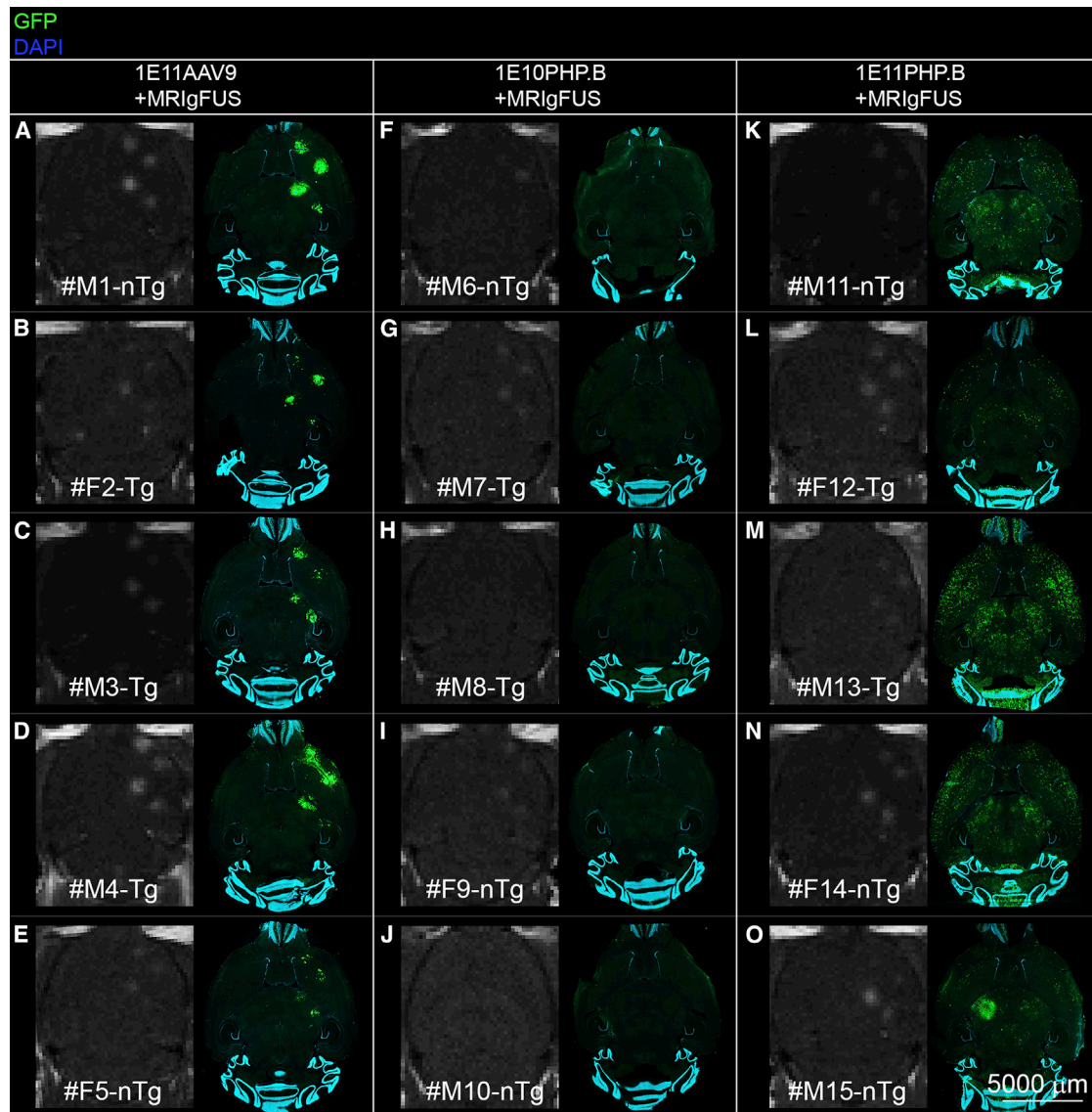
Figure 2. MRIgFUS increases the delivery of rAAV, but not PHP.B, to targeted sites in the brain

nTg and Tg mice were injected with 1E11AAV (A–E), 1E10PHP.B (F–J), and 1E11PHP.B (K–O), and MRIgFUS was used to target two spots in the cortex and striatum and two spots in the thalamus. BBB opening was confirmed by entry of the MRI contrast agent Gad. Brain sections were immunostained for GFP (green) and DAPI (teal). MR images are on the left, with corresponding stained sections on the right, representing one section for each mouse treated. 5,000 μm scale bar applies to all images.

teach MORPHIOUS the definition of microglial morphologies found in conditions without MRIgFUS exposure and AAV transduction (Figure 4P). Hereafter, areas of microglial cells that are responding to MRIgFUS and/or rAAVs were determined and defined as highly active (focal, red) or active (proximal, yellow) clusters. In mice injected with rAAV9, focal and proximal clusters were limited to areas of MRIgFUS treatment (Figure 4Q). No clusters were detected in the mice injected with 1E10 PHP.B and treated with MRIgFUS (Figure 4R). In mice injected with 1E11 GC PHP.B and treated with MRIgFUS, multiple focal and proximal clusters of microglial activation were detected throughout the brain (Figure 4S). When comparing the percentage

of total quantified area showing activated clusters, mice injected with 1E11 GC PHP.B show a significantly larger area of both focal (Figure 4T) and proximal (Figure 4U) activation compared to mice injected with 1E11 GC rAAV9 and 1E10 GC PHP.B. We then compared the IBA1 intensity in the focal (Figure 4V) and proximal (Figure 4W) clusters between viral treatment groups. We found a significantly higher IBA1 intensity in proximal clusters in animals injected with 1E11 GC PHP.B compared to animals injected with 1E11 rAAV9 (Figure 4W). We subsequently quantified the average microglial nearest neighbor distance (NND). NND corresponds to the Euclidean distance between a given microglia soma and its closest neighboring cell and
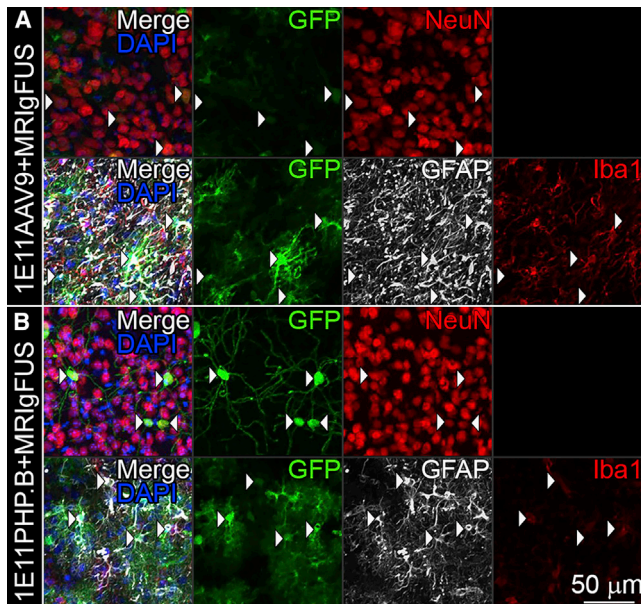
Figure 3. rAAV9 and PHP.B transduce neurons and astrocytes

Mice were treated with MRIgFUS and injected with 1E11AAV9 (A) and 1E11PHP.B (B). Brains sections were immunostained for the reporter gene GFP (green, second column), the neuronal marker NeuN (red, third column), the astrocytic marker GFAP (white, third column), and the microglial marker IBA1 (red, fourth column). Both vectors were found to transduce neurons (arrowheads, first and third rows) and astrocytes (arrowheads, second and fourth rows) but not microglia. 50 μm scale bar applies to all images.

thus, is inversely proportional to cell density. Within the proximal cluster regions of activated microglia, we saw a shorter NND in mice injected with rAAV9 compared to PHP.B (Figure 4Y). Similarly, within focal clusters, there was a tendency for a shorter NND within the rAAV9 group with p = 0.05 (Figure 4X). We saw no difference in cell size between mice injected with rAAV9 and PHP.B in either focal or proximal clusters (Figure S1). On the one hand, proximal microglial activation clusters in 1E11 GC PHP.B-injected animals showed increased IBA1 intensity, which could suggest a higher degree of activation. On the other hand, rAAV9 proximal activation clusters showed increased cell density, suggesting elevated microgliosis. Thus, based on the activation features of 1E11 GC PHP.B and rAAV9, it cannot be concluded whether individual microglia are more or less activated between 1E11 GC PHP.B and rAAV9. However, we do show that 1E11 GC PHP.B induces significantly more clusters of activated microglia throughout the brain.

The passage of rAAV9 with MRIgFUS and PHP.B to the brain triggers an immune response

We next investigated the possible association of microglial activation with an increase in MHC class II expression and the presence of T cells in the brain. Sections from mice treated with MRIgFUS and injected with 1E11 GC rAAV9, 1E10 GC PHP.B, and 1E11 GC PHP.B were immunostained for MHC class II and the T cell marker, cluster of differentiation 3 (CD3) (Figure 5). rAAV9 entry at MRIg-

FUS-targeted sites coincides with the detection of MHC class II and T cells in 70% of the MRIgFUS spots (Figures 5A and 5A1−5A5; Figures S2A−S2D). MHC class II and T cells were not observed on the contralateral side of mice treated with rAAV9 and MRIgFUS (Figures 5A and 5A1−5A5; Figures S2A−S2D) nor in MRIgFUS-targeted sites in mice treated with MRIgFUS and injected with 1E10 GC PHP.B (Figures 5B and 5B1−5B4; Figures S2E−S2H). Mice injected with 1E11 GC PHP.B and treated with MRIgFUS showed a MHC class II-positive signal and T cell infiltration at several locations in the brain, with no clear increase at MRIgFUS-targeted sites relative to other areas (Figures 5C and 5C1−5C4; Figures S2I−S2L). The T cell infiltration and MHC class II expression were seen throughout the brain following 1E11 GC PHP.B injection as visualized in a serial staining of animal #M11-nTg (Figure S3).

To better estimate the extent and variation of T cell infiltration following MRIgFUS delivery of rAAV9 and PHP.B, the number of T cells was quantified and expressed per square millimeter for each image (Figures 5D and 5E). Results indicate that, within the same mouse, there can be areas of relatively high and low T cell infiltration that could be dependent on the levels of rAAV entry following variable MRIgFUS BBB permeability for rAAV9 (Figure 5D), but this is unlikely the case for PHP.B, as MRIgFUS did not enhance delivery (Figure 5E).

The innate immune response includes the complement system that can be activated by the classical, alternative, or the lectin pathways, which all lead to the cleavage and activation of the complement component C3.[35] It has been suggested that the complement system plays a role in the induction of a humoral response following rAAV injections in mice.[32] To investigate the complement system following the entry of rAAV9 and PHP.B to the brain, sections were immunostained for complement component C3d. C3d is bound to tissue surfaces upon complement component C3 cleavage and can be used to measure complement activation retrospectively.[35] In mice injected i.v. with 1E11 GC rAAV9, a C3d complement activation response, determined as positive C3d staining, was observed in 50% of the MRIgFUS spots and not in the contralateral hemisphere (Figures 6A and 6A1−6A5; Figures S4A−S4D). The i.v. injection of 1E10 GC PHP.B combined with MRIgFUS did not induce detectable complement activation (Figures 6B and 6B1−6B4; Figures S4E−S4H); however, 1E11 GC PHP.B induced complement activation throughout the brain (Figures 6C and 6C1−6C4; Figures S4I−S4L). The complement activation in both 1E11 GC rAAV9- and 1E11 GC PHP.B-injected mice was seen in proximity to vessels (Figures 6A4, 6A5, 6C1, and 6C3). These results indicate that the passage of rAAV9 and PHP.B from the blood to the brain parenchyma induces an activation of the complement system especially around vessels, which is not induced by MRIgFUS alone when rAAV doses are too low for transduction of brain cells.

MRIgFUS increases both rAAV9 and PHP.B delivery to the brain in BALB/c mice

Primates do not express the Ly6A receptor, and therefore the PHP.B is unable to cross the BBB to a higher extent than rAAV9 in humans.[36] However, in the original publication describing the PHP.B
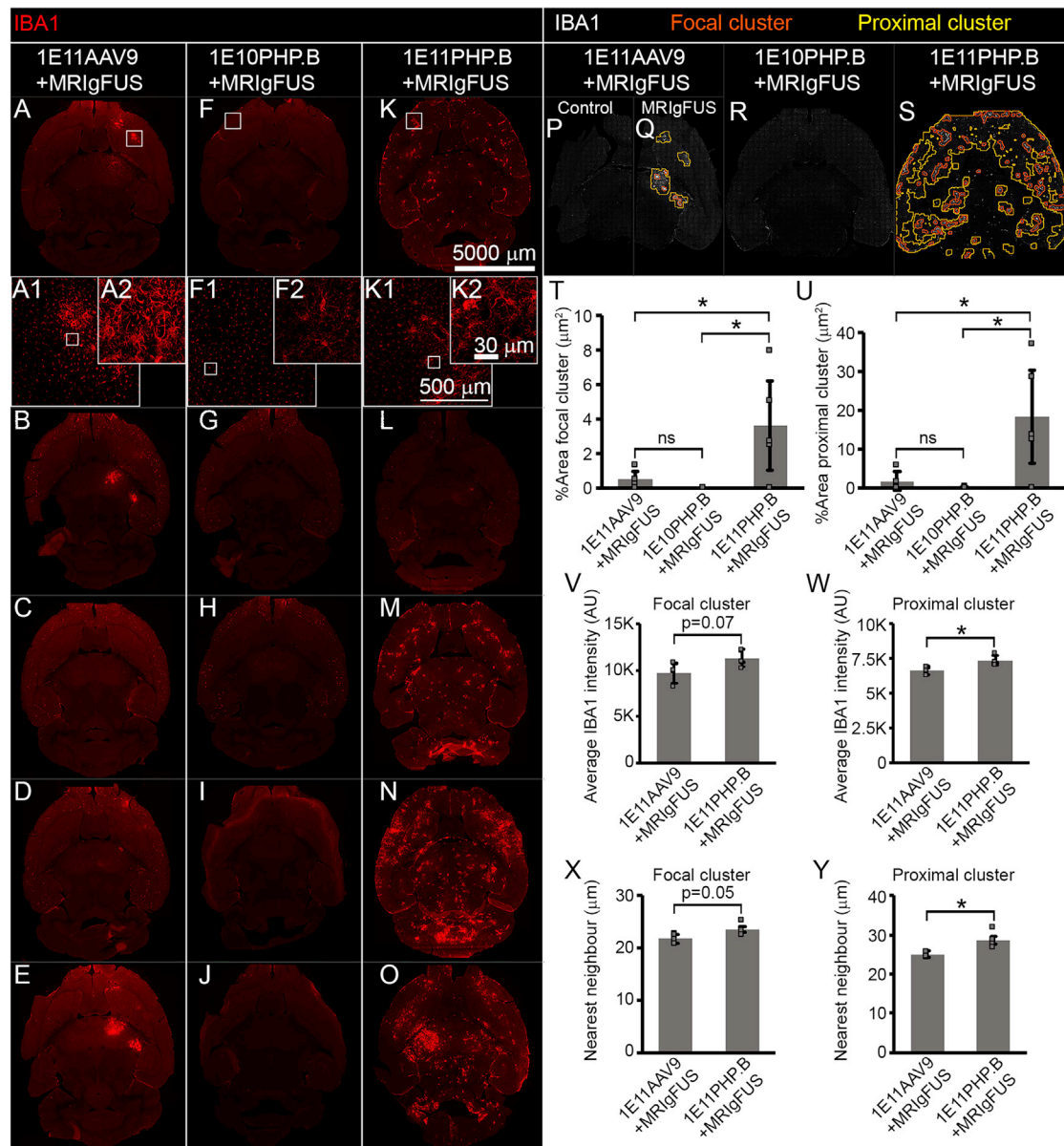
Figure 4. Microglia activation following MRIgFUS-rAAV9 delivery and i.v. administration of PHP.B

nTg and Tg mice were injected i.v. with 1E11AAV9 (A–E), 1E10PHP.B (F–J), and 1E11PHP.B (K–O) and treated with MRIgFUS. Sections were immunostained with IBA1, a marker of microglia and macrophages. Pictures from individual mice are displayed in the same order as in Figure 2. (A1), (F1), and (K1) correspond to insets in (A), (F), and (K), respectively. (A2), (F2), and (K2) correspond to insets in (A1), (F1), and (K1), respectively. For analysis of microglial activation, the contralateral, non-MRIgFUS-treated hemisphere of mice injected with 1E11AAV9 was used as control (P). Focal (red) and proximal (yellow) clusters of activated microglia were hereafter identified in the MRIgFUS-treated hemisphere of mice injected with 1E11AAV9 (Q), as well as in mice treated with MRIgFUS and injected with 1E10PHP.B (R) and 1E11PHP.B (S). Mice injected with 1E11PHP.B had a significantly larger area of focal (T) and proximal (U) clusters compared to mice injected with 1E11AAV9 and 1E10PHP.B. In mice injected with 1E11AAV9 and 1E11PHP.B, average IBA1 intensity (V and W) and distance to the nearest neighbor (X and Y) were measured in focal and proximal clusters. Statistical comparisons were performed using Student's unpaired t test for comparison of two groups and one-way ANOVA followed by Sidak's post hoc test for comparison of multiple groups. Results are displayed with bars representing mean ± standard deviation, *p < 0.05 (P and Q). 5,000 μm scale bar (K) applies to (A–O); 500 μm scale bar (K1) applies to (A1), (F1), and (K1); and 30 μm scale bar (K2) applies to (A2), (F2), and (K2).

vector, it was demonstrated that PHP.B transduces a higher number of astrocytes and neurons than rAAV9 in human-induced pluripotent stem cell-derived cortical spheroids.[9] This finding suggests that

PHP.B may still result in a higher transduction efficiency in non-Ly6A-expressing brain tissue, provided that the vector can cross the BBB. BALB/c mice express low levels of one of the Ly6A receptor
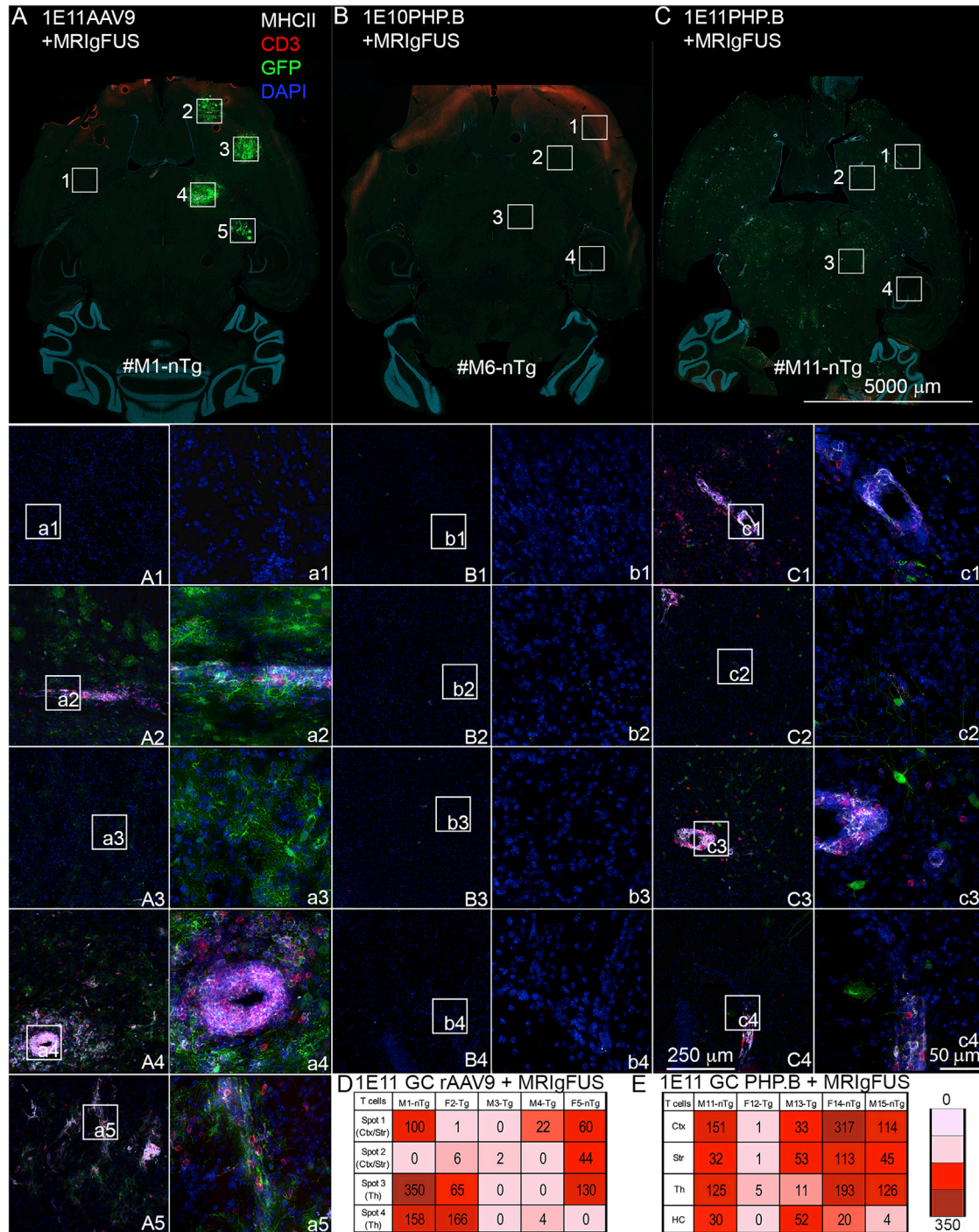
Figure 5. The entry to the brain of rAAV9 with MRIgFUS and PHP.B coincides with markers of an adaptive immune response

Brain sections were immunostained for MHC class II, the T cell marker CD3, and GFP following treatment with MRIgFUS and injection of 1E11AAV9 (A), 1E10PHP.B (B), and 1E11PHP.B (C). Insets in (A), (B), and (C) correspond to (A1−A5), (B1−B4), and (C1−C4), respectively. Insets in (A1−A5), (B1−B4), and (C1−C4) correspond to (a1−a5), (b1−b4), and (c1−c4), respectively. T cell infiltration and MHC class II expression are visible in MRIgFUS spots in animals injected with rAAV9 but not in the contralateral site and in multiple brain areas in animals injected with 1E11PHP.B but not 1E10PHP.B. MHC class II expression is primarily seen around large vessels, and T cells also infiltrate

(legend continued on next page)

variants (V106A), resulting in very limited, if any, binding and uptake of PHP.B from the blood to the brain.[17] To investigate the efficacy of MRIgFUS-mediated delivery of PHP.B to the brain in animals with reduced Ly6A-mediated PHP.B BBB uptake, 1E11 GC of i.v. PHP.B was used in BALB/c mice and compared to rAAV9.[16] MRIgFUS targeted 2 spots in the cortex/striatum and 2 spots in the thalamus of BALB/c mice, as previously done in the Tg mouse strain (Figure 1). Increased BBB permeability observed by Gad enhancement, as well as GFP expression 3 weeks following treatment in MRIgFUS-targeted spots, was observed both in mice injected with rAAV9 (Figure 7A) and PHP.B (Figure 7B). No differences between groups were observed for Gad enhancement (Figure 7C) and ultrasound pressure (Figure 7D).

Brain sections were immunostained for GFP (green), DAPI (teal), the neuronal marker (NeuN; red),[37,38] and the astrocytic marker, S100 calcium-binding protein (S100B; white).[39,40] Images were acquired of the 1-mm-diameter MRIgFUS spots (Figure 7E), and GFP-positive neurons (Figure 7E; arrow) and GFP-positive astrocytes (Figure 7E; arrowhead) were quantified using Cell Profiler. The percentage of double GFP- and NeuN-positive (GFP$^+$/NeuN$^+$) cells out of the total number of NeuN$^+$ cells describes the percentage neuronal transduction (Figure 7F). There was no significantly different neuronal transduction efficiency between rAAV9 and PHP.B delivered with MRIgFUS in BALB/c mice, although there was a trend toward a higher neuronal transduction in mice injected with rAAV9 (p = 0.07). Similarly, the percentage of GFP$^+$ and S100B-positive (GFP$^+$/S100B$^+$) cells out of the total number of S100B$^+$ cells describes the percentage astrocytic transduction (Figure 7G). There was a significantly higher astrocytic transduction in BALB/c mice injected with rAAV9 and treated with MRIgFUS than in mice injected with PHP.B and treated with MRIgFUS (Figure 7G). These results demonstrate that when both vectors are allowed to cross the BBB using MRIgFUS in the BALB/c mouse strain, PHP.B does not lead to a higher transduction efficiency in the brain compared to rAAV9, as previously shown to be the case by others *in vitro* in human-derived neuronal cultures.[9]

DISCUSSION
Efficacy of MRIgFUS rAAV9 and PHP.B delivery to the brain and transduction patterns
Gene therapy is promising for the treatment of neurodegenerative disorders, including AD. Here, we established in a mouse model of amyloidosis that a relatively low i.v. dose of 1E11 GC rAAV9 combined with MRIgFUS, or using the PHP.B capsid, results in non-invasive gene delivery to the brain of males and females Tg and nTg mice. Based on the knowledge that clinical trials reported, with the possibility that high vector dosage can trigger an immune reaction to rAAVs and to the transgene being expressed,[7] we aimed to determine whether the enhanced ability of PHP.B to transduce the brain could be achieved at relatively low i.v. dosage when combined with MRIgFUS. However, MRIgFUS delivery of PHP.B, administered i.v. at 1E10 GC, did not result in the transduction of brain cells in the MRIgFUS-targeted spots. Moreover, at a dose of 1E11 GC, PHP.B cell transduction was widespread in the brain and was not enhanced at MRIgFUS spots. These results indicate that a critical concentration of PHP.B i.v. is required for efficient BBB crossing and subsequent transduction in animals expressing high levels of the Ly6A receptor and that this threshold was not reduced at sites of MRIgFUS-induced BBB permeability.

One study reported preliminary data on gene delivery to C57BL/6 mice using PHP.B at 1E11 GC i.v. in combination with MRIgFUS, and the results suggested an increase in PHP.B delivery to MRIgFUS-targeted sites,[41] in contrast to our findings. However, only one high-magnification image was shown to corroborate this statement, and based on our experience, the resulting patchy transduction pattern in the brain with PHP.B (Figure 2) requires a thorough evaluation across entire brain sections to properly assess whether consistent increases in transgene expression are found at MRIgFUS-targeted areas. In our hands, PHP.B led to a variable and widespread transduction and transgene expression in the brain of Tg mice, irrespective of the MRIgFUS spots. In contrast, rAAV9 delivered by MRIgFUS transduced cells only in targeted regions where high transgene expression was found.

The ability of PHP.B to deliver gene therapies non-invasively to cells throughout the brain holds promise for validation of therapeutics aimed to target pathologies affecting multiple brain areas at once, for example, at disease stages where toxic Aβ peptides are present in several brain regions. The PHP.B construct could be modified with a GFAP promoter to control therapeutic transgene expression in response to astrocytic activation triggered by, for example, Aβ pathology.[15] In contrast, MRIgFUS-mediated delivery of rAAV9 allows for a more targeted delivery of therapeutics to a subset of neurons or brain areas, which is of relevance for the treatment of regional AD-related pathologies at early disease stages and dysfunctions of localized cell populations, e.g., cholinergic neurons in the basal forebrain.[27]

In contrast to rAAV9, MRIgFUS only enhances brain delivery of PHP.B in animals with reduced Ly6A receptor expression
Previous studies have demonstrated an increased transduction of human-derived, induced pluripotent stem cells when using PHP.B compared to rAAV9.[9] This suggests that PHP.B may result in a higher transduction efficiency of human brain tissue compared to rAAV9. However, it is also recognized that PHP.B may not cross the BBB in humans because of the lack of its cognate receptor, Ly6A, in primates.[16,20] To investigate whether MRIgFUS can overcome this

---

into the brain parenchyma. The number of T cells per square millimeter is displayed for each mouse and each MRIgFUS spot (for rAAV9; D) or brain area (for PHP.B; E). Quantifications show variability in T cell invasion within and between mice in both groups, as well as T cell invasion in all brain areas quantified in mice injected with 1E11PHP.B. Ctx, cortex; Str, striatum; Th, thalamus; HC, hippocampus. 5,000 μm scale bar (C) applies to (A−C), 250 μm scale bar (C4) applies to (A1−C4), and 50 μm scale bar (c4) applies to (a1−c4).

limitation and potentially enable the use of PHP.B in animals and humans devoid of the Ly6A receptor, we evaluated the delivery of PHP.B to the brain of BALB/c mice using MRIgFUS. In contrast to the findings in the Tg mouse strain, where MRIgFUS could not increase the brain delivery of PHP.B, MRIgFUS was able to deliver the PHP.B vector to the brain of BALB/c mice, albeit at lower transduction efficiency than rAAV9. These findings suggest that the BBB permeability created by MRIgFUS can be utilized for the delivery of the PHP.B vector in some mouse strains but not in others. We hypothesize that the high levels of Ly6A receptor expression on the brain vasculature in C57BL/6-derived mouse strains, such as Tg mice, effectively capture the PHP.B, rendering the PHP.B levels in circulation insufficient to pass the BBB through MRIgFUS-targeted sites. In BALB/c mice, a combination of reduced expression and affinity of the V106A Ly6A receptor variant limits receptor-mediated brain uptake of i.v. PHP.B,[17] thereby allowing the vector to enter sites of MRIgFUS-induced BBB permeability. Compared to rAAV9, however, brain transduction of PHP.B following MRIgFUS-mediated delivery in BALB/c mice is lower. This suggests that PHP.B is hindered, to a greater extent than rAAV9, in its ability to cross the BBB at MRIgFUS-targeted sites. This could be caused by the remaining, although low, binding to the V106A Ly6A receptor. Further investigations are warranted to determine underlying mechanisms.

Immune response to MRIgFUS-delivered rAAV9 and PHP.B

The immune response to rAAVs is generally considered low,[42] although both humoral and cellular responses are seen in preclinical and clinical research.[43] i.v. injection of rAAV9 has shown an excellent safety profile and ability to deliver genes across the blood-CNS barriers when injected i.v., leading to US Food and Drug Administration (FDA) approval of rAAV9 as a gene carrier in a gene-therapy treatment for spinal muscular atrophy in children.[44] The PHP.B vector enables gene delivery to the brain at lower i.v. doses than rAAV9,[9] and it was found that PHP.B does not induce a humoral response upon i.v. injection in 2-week-old mice.[45] High-dose i.v. injections of rAAVs are, however, not harmless, and one study has reported serious complications and liver toxicity after injection of 7.5E13 GC/kg PHP.B, but not rAAV9, in rhesus macaques.[20] Additionally, the recent deaths in the ASPIRO trial using i.v. injections of rAAV8 further highlight the need for new strategies to achieve safe gene delivery without high rAAV doses. MRIgFUS can increase the delivery of rAAV to the brain, and MRIgFUS treatment without rAAV delivery results in a benign microglial activation, which resolves after 15 days.[46] No study has yet investigated the immune response following rAAVs delivery to the brain using MRIgFUS.

The immune response following intracranial injections of rAAVs has been studied in detail, demonstrating that this can lead to microglial activation, MHC class II expression, T cell infiltration, and activation of the complement system.[28–33] A cytotoxic T cell response can be directed against rAAV-transduced cells, triggering their elimination.[47] As transduced cells die, the expression of therapeutic transgenes severely decreases, compromising the clinical benefits of rAAV-based gene therapies,[33] and in the brain, resulting in a loss of irreplaceable neurons.[30,31] In clinical trials, gene delivery by rAAVs

can cause an immune response both toward the rAAV capsid and the expressed transgene. However, cytotoxic T cell responses targeting the rAAV capsid are not seen in preclinical models in the absence of intervention, where T cell responses are instead directed toward the transgene expression.[33]

Here, we investigated markers of immune reaction in the brain when delivering GFP, a non-self protein, under control of a ubiquitous promoter using PHP.B- or MRIgFUS-mediated delivery of rAAV9 in a mouse model of AD.

Our data show that in both Tg and nTg, males and females, 1E11 GC PHP.B and 1E11 GC rAAV9 delivered by MRIgFUS led to microglial and complement system activation, as well as an adaptive immune response based on increased MHC class II expression and T cell infiltration in the brain. With rAAV9, the immune response was limited to MRIgFUS-targeted sites, whereas with PHP.B, it was absent at low dose where no brain cell transduction occurred and widespread at a high dose. This suggests that the immune response is caused by the transduction of cells with rAAVs and the subsequent transgene expression and not by the disruption of the BBB caused by MRIgFUS.

Decreasing the immune response for gene delivery with PHP.B and MRIgFUS-rAAV9

In animal models, including rodents and non-human primates, it is generally accepted that T cell responses toward the rAAV capsid are not seen.[33] In contrast, T cell infiltration and MHC class II expression can occur when non-self proteins such as GFP are expressed by astrocytes and microglia.[48] For example, an adaptive immune response was observed following intracranial injections of rAAV9, modifying astrocytes and neurons to express GFP or human aromatic l-amino acid decarboxylase (both non-self proteins in the animal models), but not when rAAV2 was used to primarily render neurons capable of producing the proteins.[28,29] Here, PHP.B- and MRIgFUS-delivered rAAV9 transduce both astrocytes and neurons, corroborating what others have found following i.v. injections of PHP.B and using MRIgFUS-mediated delivery of rAAV9.[8,9] Specifically, previous studies have demonstrated that cells transduced following MRIgFUS-mediated delivery of rAAV9 are between 36% and 63% astrocytes and 18% and 58% neurons depending on the brain area.[8] At the same dose as used in the current study (1E11 GC/mouse), PHP.B has been shown to transduce between 40% and 50% of the neurons and 30% and 70% of the astrocytes, again with differences attributed to brain regions.[49] Therefore, in our study, the T cell infiltration and MHC class II expression observed are likely triggered by the expression of GFP by glial cells. An adaptive immune response could eventually cause loss of transgene-expressing neurons even when originating from glial cells.[28] At the same time, T cell responses can also induce tolerance to the foreign transgenes through activation of regulatory T cells, especially following gene transfer to the liver.[50]

The current study investigated a single time point, which limits the evaluation of the immune response over time and the effects that it may have on transgene expression. An adaptive immune response
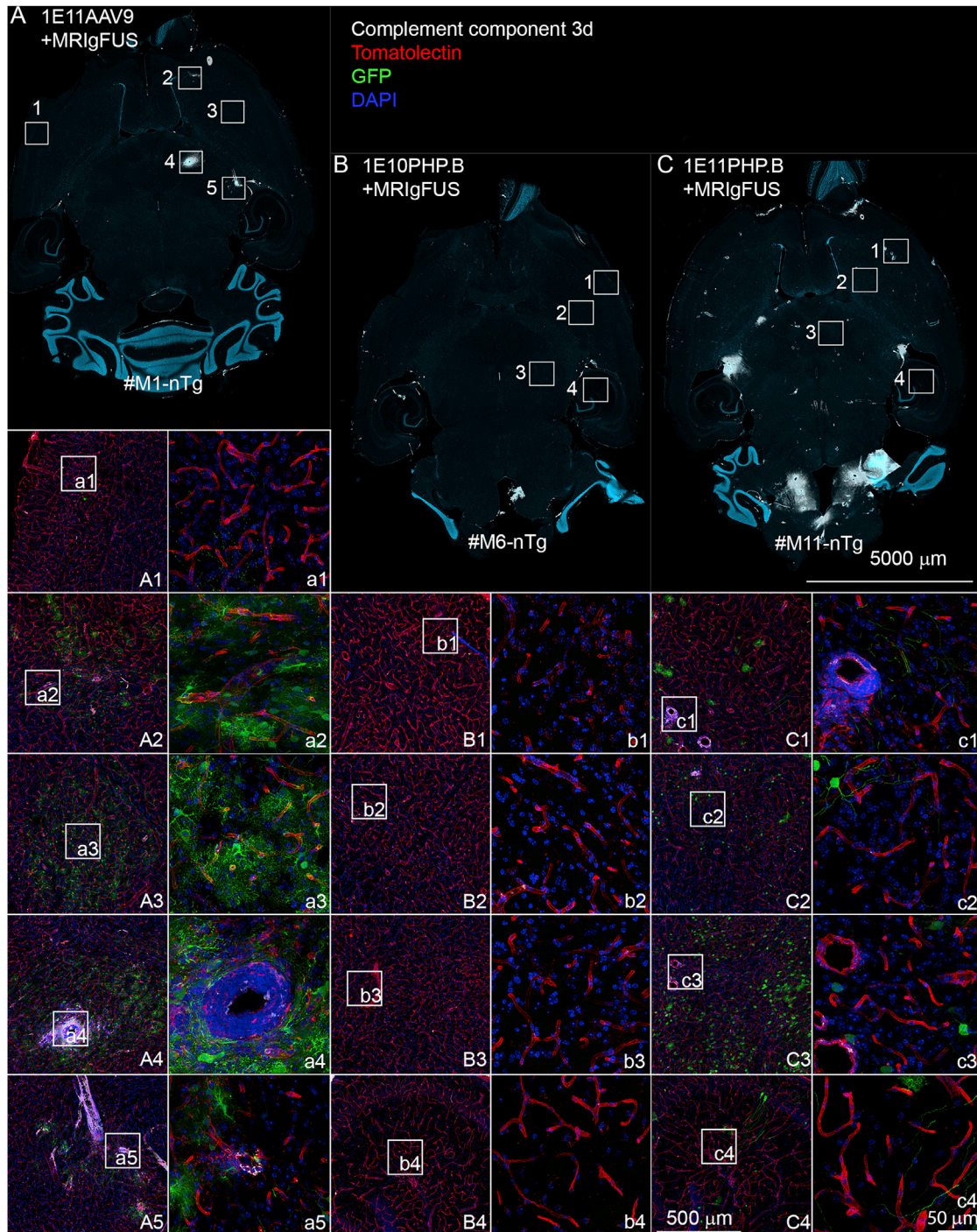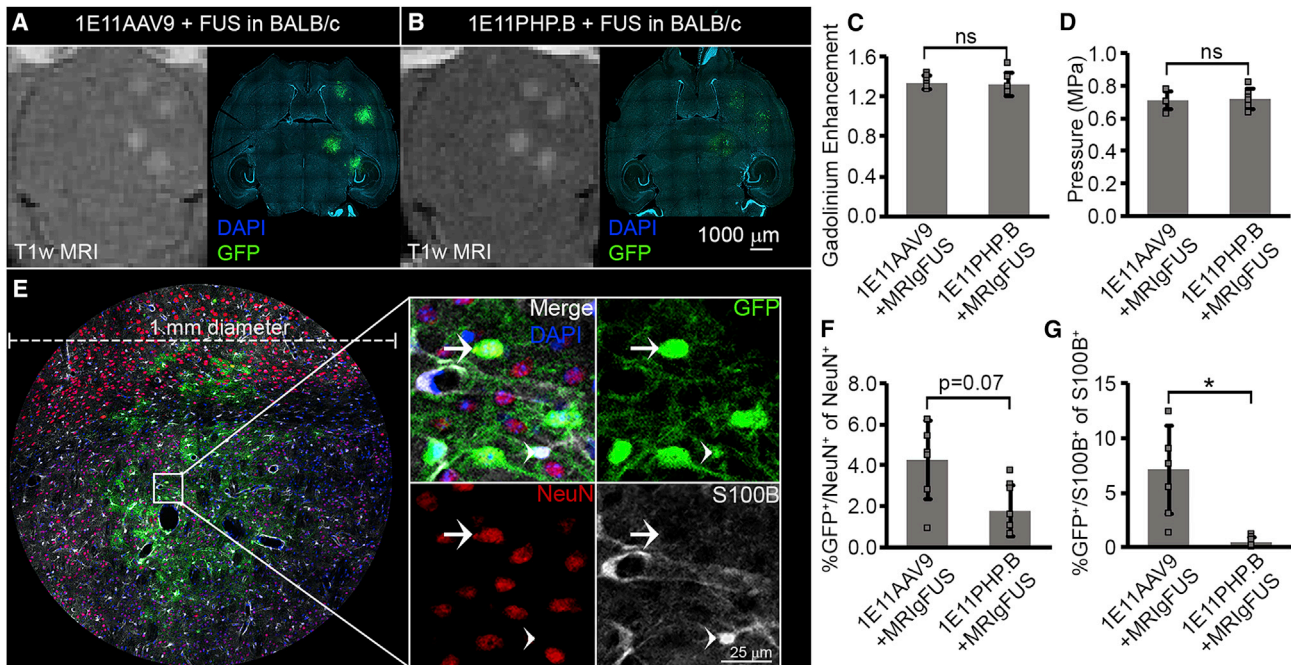
Figure 6. The entry of rAAV9 delivered by MRIgFUS and PHP.B in the brain induces complement activation around blood vessels

Mice were injected with 1E11AAV9 (A), 1E10PHP.B (B), and 1E11PHP.B (C) and treated with MRIgFUS. Brain sections were immunostained for the complement component C3d (white), the vessel marker tomato lectin (red), and GFP (green). Insets in (A), (B), and (C) correspond to (A1−A5), (B1−B4), and (C1−C4), respectively. Insets in (A1−A5), (B1−B4), and (C1−C4) correspond to (a1−a5), (b1−b4), and (c1−c4), respectively. 5,000 μm scale bar (C) applies to (A−C), 500 μm scale bar (C4) applies to (A1−C4), and 50 μm scale bar (c4) applies to (a1−c4).

Figure 7. MRIgFUS enhances brain delivery of both rAAV9 and PHP.B in BALB/c mice

BALB/c mice were injected with 1E11AAV9 (A) and 1E11PHP.B (B) and treated with MRIgFUS targeting two spots in the cortex/striatum and two spots in the thalamus, as previously done in the Tg mouse strain (Figures 1A−1C). 3 weeks following the treatment, animals were sacrificed, and brain sections were immunostained for GFP (green) and DAPI (teal) (A and B). Gad enhancement (C) and applied ultrasound pressure (D) were quantified in mice injected with rAAV9 (n = 6) and PHP.B (n = 6). Brain sections were immunostained for GFP (green), DAPI (teal), the neuronal marker NeuN (red), and the astrocytic marker S100B (white), and images of each of the four 1-mm-diameter ultrasound spots were acquired. Example of a 1-mm-diameter image used for Cell Profiler quantifications from MRIgFUS spot in the striatum of rAAV9-injected animals (E). Colocalization between GFP and NeuN (E; arrow) and GFP and S100B (E; arrowhead) was quantified. Percentage neuronal transduction was determined as percentage double GFP- and NeuN-positive (GFP$^+$/NeuN$^+$) out of total number of NeuN$^+$ cells (F). Similarly, percentage astrocytic transduction was determined as percentage GFP$^+$ and S100B-positive (GFP$^+$/S100B$^+$) out of total number of S100B$^+$ cells (G). Statistical analyses were performed using Student's t test. Bars represent mean ± standard deviation, *p < 0.05. 1,000 μm scale bar (B) applies to (A and B), and 25 μm scale bar applies to squared images in (E).

toward the transgene can lead to loss of transduced cells and transgene expression,[47] with the degree to which this is occurring depending on the transgene, the animal model, and the brain region. For example, rAAV-mediated delivery of genes encoding GFP has led to cell loss in both rodents and non-human primates, initiated approximately 1 month post-rAAV administration.[29,31,47] In rodents, delivery of genes encoding either progranulin or human aromatic L-amino acid decarboxylase induced a stronger immune response with a more pronounced cell loss than genes encoding GFP.[29,31] In contrast, in non-human primates, cell loss following transgene GFP expression has been reported, but a minimal immune response toward human aromatic L-amino acid decarboxylase was seen, likely because of the 97% homology between human and non-human primate aromatic L-amino acid decarboxylase.[28] Finally, intracranial delivery of a gene encoding progranulin induced cell loss, primarily in the mouse hippocampus but not in the striatum or cortex despite transgene expression in all three brain areas.[31] The immune response to human primate aromatic L-amino acid decarboxylase in rats resulted in cell loss in both striatum and thalamus,[29] and similarly, GFP expression in non-human primates led to cell loss in both striatum and cortex.[28] It remains unclear why some brain regions are

more susceptible to cell loss than others following transgene expression. The long-term effects of the immune response toward therapeutic genes delivered using the non-invasive delivery methods used in the current paper should thus be assessed for each transgene and brain region, across multiple animal models, to determine the safety and long-term stability of the transgene expression.

The strong neuronal tropism of rAAV2 and its modest impact on the immune system[28,29] make this serotype attractive for clinical applications and for MRIgFUS delivery.[12,14,15] To limit the immune reaction caused by PHP.B, its tropism could be modified to restrict glial transduction and/or by using a neuron-specific promoter to drive transgene expression mainly in this cell population. This is supported by the prevention of a humoral immune response using liver, muscle, or neuron-specific promoters to avoid transgene expression in professional antigen-presenting cells.[51] A neuron-specific promoter, such as the synapsin promoter, could therefore be used to specifically favor transgene expression in neurons and thereby reduce the potential of an immune response and ensure long-term transgene expression upon gene delivery to the brain either using PHP.B or rAAV delivered by MRIgFUS.[14,52–55]

Conclusions

PHP.B, or rAAV9 combined with MRIgFUS to modulate the BBB, can be used to deliver transgenes to the brain non-invasively, i.e. without the need for intracranial surgeries, in the Tg mouse model of amyloidosis. In the current experimental design, the attempt to use MRIgFUS delivery to reduce the i.v. dose of PHP.B required for the transduction of brain cells was unsuccessful in Tg mice. The two successful delivery approaches, namely (1) i.v. PHP.B and (2) i.v. rAAV9 combined with MRIgFUS, at the same viral dose resulted in distinct transgene distributions, which can be utilized for future investigations of therapeutic transgenes that may require a widespread or targeted delivery to the brain, respectively. In the Tg mouse model, the delivery of i.v. PHP.B, or rAAV9 combined with MRIgFUS, to the brain results in an immune response characterized by increased MHC class II expression, T cell invasion, and microglial activation. Future gene therapy studies for the treatment of neurodegenerative disorders can be tailored to limit the immune response, for example by directing rAAVs toward neuronal transduction and expression.

MATERIALS AND METHODS

Mice

Fifteen male and female Tg mice and nTg littermates were used in this study, with details on individual mice described in Table 1. The Tg mouse strain is a C57BL/6 and C3H hybrid expressing human amyloid precursor protein 695 harboring the Swedish (KM670/671NL) and the Indiana (V717F) mutations under the hamster prion promoter and developing Aβ plaques by 3 months of age.[23] Twelve wild-type BALB/c male and female mice were also used in this study. Animals were provided with food and water *ad libitum* and kept in a 12-h light/dark cycle at 18°C−22°C and 40%–60% humidity. All animal work was performed according to the Canadian Council on Animal Care Policies & Guidelines and Animals for Research Act of Ontario and was approved by the Sunnybrook Research Institute Animal Care Committee.

rAAV constructs

The rAAV genome plasmid (pEMS2143) used here has also been used previously[56,57] and is available from Addgene (www.addgene.org). In brief, it is ssAAV-smCBA-EmGFP-WPRE, where ssAAV is single-stranded AAV, smCBA is a smCBA enhancer chosen for ubiquitous expression,[25,56–58] EmGFP is used,[59] and WPRE is the 3′ UTR woodchuck hepatitis virus post-transcriptional regulatory element mut6.[60,61] For this work, pEMS2143 was packaged into either rAAV9 or PHP.B by the University of Pennsylvania Vector Core (Philadelphia, PA, USA).[9,62] Virus was provided by the Vector Core at titers of 6.12E13 GC/mL for rAAV9 and 2.96E13 GC/mL for PHP.B by droplet digital polymerase chain reaction (ddPCR) in phosphate-buffered saline (PBS) with 0.001% pluronic acid.

All vectors were diluted in sterile PBS (Wisent; 311-010-CL) to a total volume of 100 μL per i.v. injection. rAAV9 and PHP.B were injected through tail-vein catheters (see MRIgFUS procedure), and all GC doses are stated as per an average 30-g mouse and were adjusted to the weight of each individual mouse to ensure equal rAAV dose per gram mouse.

MRIgFUS procedure

For a detailed description of MRIgFUS-mediated delivery of rAAV, see Noroozian et al.[63] and Touahri et al.[64] Mice were anesthetized using isoflurane and prepared for MRIgFUS by placing an angiocatheter in the tail vein and removing all hair from the animal's head to properly couple the skin to the transducer, without air pockets. Mice were thereafter placed in a supine position on an MRI-compatible sled, and pre-sonication T1w and T2w scans were acquired using a 7.0-T MRI (BioSpin 7030; Bruker, Billerica, MA, USA). T2w scans were used for targeting of the ultrasound's foci to the cortex/striatum and the thalamus. Targeting the thalamus also leads to ultrasound treatment of the ventral hippocampus, as the ultrasound beam does not have the spatial resolution in the z axis to specifically target the thalamus only. This paper will hence forth focus on the thalamus only and not the ventral hippocampus. An in-house manufactured focused ultrasound (FUS) system (the prototype of RK100 focused ultrasound system; FUS Instruments, Toronto, ON, Canada), was used and ultrasound waves were generated by a 1.68- to 1.78-MHz spherically focused transducer (75 mm diameter, 60 mm radius of curvature, 7 cm aperture, F-number: 0.8). Focused ultrasound was applied for 120 s in 10 ms bursts with a frequency of 1 Hz; 0.02 mL/kg Definity microbubbles (Lantheus Medical Imaging, North Billerica, MA, USA) were injected through the angiocatheter simultaneously with the initiation of focused ultrasound. A 4.8-mm-diameter wideband polyvinylidene fluoride hydrophone was located in the transducer, and the pressure was gradually increased until sub-harmonic emissions were detected, verifying stable cavitation of the microbubbles without inertial cavitation/bursting of the microbubbles. The pressure was hereafter continued at 50% of the sub-harmonic detection levels, which have previously been shown to induce increased BBB permeability without tissue damage.[65] rAAV was injected through the angiocatheter immediately after detection of microbubble cavitation ensuring optimal BBB permeability at the time of injection. The MR contrast agent Gad (Omniscan; GE Healthcare Canada, Mississauga, ON, Canada) was injected after rAAV injection at a dose of 0.2 mL/kg. T1w scans were performed immediately after sonication to visualize BBB permeability by entry of Gad into the brain (Figures 1 and 7).

Quantification of Gad contrast

MR images were opened in Medical Image Processing, Analysis, and Visualization (MIPAV). A 1 × 1-mm square was placed over each MRIgFUS spot and in the contralateral hemisphere (Figure 1), and average intensity within each square was measured. Average intensity in MRIgFUS spots was divided by average intensity in the contralateral hemisphere, and the mean of the four MRIgFUS spots in each mouse was used for statistical comparisons.

Tissue processing and staining

3 weeks following MRIgFUS treatment and rAAV i.v. injection, mice were sacrificed by transcardial perfusion of deeply anesthetized mice using intraperitoneal-injected 75 mg/kg ketamine and 10 mg/kg xylazine. Mice were perfused with 0.9% saline followed by 4% paraformaldehyde in 0.1 M PO₄, after which, whole-brain dissections were

performed. Brains were post-fixed overnight in 4% paraformaldehyde in 0.1 M PO$_4$ followed by incubation for a minimum of 48 h in 30% sucrose in 0.1 M PO$_4$. The tissue was mounted on a sliding microtome using Tissue-Tek Optimal Cutting Temperature (Sakura, Torrance, CA, USA) and frozen with dry ice for 30 min before sectioning into 40 μm-thick sections. Sections were stored in cryoprotective glycerol solution at −20°C.

Free-floating sections were processed for staining in multi-well plates. Sections were washed 3 times for 10 min in 0.5 mL PBS. All staining with the exception of GFP and IBA1 was enhanced by antigen retrieval for 60 min (30 min for S100B) at 70°C in 10 mM Tris base supplemented with 0.05% v/v Tween 20 and 1 mM EDTA (pH 9). Following antigen retrieval, sections were washed 3 times for 10 min in PBS and blocked for a minimum of 2 h in 200 μL blocking buffer (PBS supplemented with 0.3% Triton X-100, 3% w/v bovine serum albumin, and 10% v/v donkey serum). Sections were incubated with primary antibodies in 200 μL blocking buffer at 4°C for 24 h (Figures 4 and 7; Figure S3) and 72 h (all other figures), followed by 3, 10-min washes in PBS, and incubated with secondary antibodies in 200 μL blocking buffer overnight, followed by a 10-min incubation in PBS with DAPI. Finally, sections were washed twice in PBS for 10 min and again washed in 0.1 M PO$_4$ for 10 min. Sections were then mounted on glass slides in polyvinyl alcohol mounting medium with 1,4-diazabicyclo2.2.2octane (DABCO) (Millipore; 10981) and covered with glass coverslips. Primary antibodies and dilutions included the following: rabbit anti-GFP 1:1,000 (Millipore; AB3080), chicken anti-GFP 1:1,000 (Abcam; ab13970), Guinea pig anti-NeuN 1:500 (Millipore; ABN90), rabbit anti-IBA1 1:500 (Wako; 016-20001), goat anti-GFAP 1:1,000 (Novus Biologicals; NB100-53809), rabbit anti-S100B 1:800 (Abcam; ab41548), goat anti-complement component C3d 1:200 (R&D Systems; AF2655), tomato lectin 1:200 (Vector Laboratories; B-1175), rabbit anti-CD3 1:200 (Abcam; ab16669), and rat anti-MHC class II 1:200 (Invitrogen; 14-5321-82). All secondary antibodies were purchased from Jackson ImmunoResearch Laboratories and diluted 1:400.

Imaging and quantifications

Whole section images were acquired using Zeiss Axio Scan.Z1, except for whole section images of IBA1 used for quantifications in Figure 4, which was acquired as z stack images on a Zeiss Z1 Axio Observer confocal spinning disk. All other images were acquired as z stacks using a Zeiss Z1 Axio Observer confocal spinning disk and are presented as maximum intensity projections, except for single-plane images acquired for quantification with Cell Profiler (Figure 7).

CD3-positive cells, indicative of T cell invasion, were counted per square millimeter on all images displayed in Figure 6. MHC class II expression and CD3-positive cells were either clearly present or absent in MRIgFUS spots, as illustrated in Figure S2. z stack 20× images from each spot were used to evaluate MHC class II expression and T cell invasion and revealed that such events were detected in 70% of the MRIgFUS spots. Similarly, complement component C3d staining was noticed in 50% of the MRIgFUS spots.

IBA1 fluorescence intensity and morphological analysis

We identified activated microglia using MORPHIOUS, a recently developed machine-learning method (manuscript deposited in bioRxiv).[34] In brief, MORPHIOUS learns the definition of a microglial morphology from control tissues not activated by MRIgFUS or rAAV transduction and from this definition, infers regions of interest corresponding to non-normal or activates microglia in treated tissues. Microglial clusters identified as activated are divided into focal and proximal clusters depending on the degree of activation, with focal clusters harboring the highest degree of activation. Two whole-brain sections from each mouse were used to measure microglial activation. Sections from 5 mice injected with rAAV9 and treated with MRIgFUS were divided into the ipsilateral and contralateral hemisphere, and the contralateral sections were used to train the MORPHIOUS software.

In sections immunostained with IBA1, a marker of microglia and macrophages, morphological features related to IBA1 fluorescence, soma characteristics, and skeleton complexity were quantified using custom ImageJ scripts, as described in detail in a manuscript deposited in bioRxiv.[34] In brief, images were first post-processed using the subtract background command (radius = 50) and the local contrast-enhanced command (blocksize = 127, histogram = 256, maximum = 2.5) and despeckled. A local threshold was applied to the images (auto-local threshold: method = Phansalkar, parameter 1 = 0, parameter 2 = 0) to delineate IBA1 foreground pixels, and the IBA1 intensity was measured. Subsequently, images were binarized and skeletonized, and skeletal features (i.e., branch length, number of branches, etc.) were measured (command: Analyze Skeleton [2D/3D]).

Microglia cell bodies were delineated and counted using a custom ImageJ script, which we are describing in detail in a manuscript deposited in bioRxiv,[34] based on the ImageJ MorphoLibJ package.[66] In a slight modification to the original method, images were first local contrast enhanced (slope = 2.0). We calculated the mean skeletal features per cell by normalizing whole-image skeletal features to the number of microglia bodies in an image. For each microglial cell body, the Euclidean distance ($d = \sqrt{(x_2 - x_1)^2 - (y_2 - y_1)^2}$) to each other microglial cell body was evaluated. Thereafter, the NND was determined as the distance between a microglia and its closest neighboring cell. The NND for all microglia within a given region (i.e., focal or proximal cluster region) was averaged together. The NND was calculated using a custom Python script (see detailed description in manuscript deposited in bioRxiv).[34]

Proximally activated microglia were identified using the microglial features area, mean intensity, fractal dimension (D), number of cells, NND, soma size, soma circularity, number of branches, branch length, number of branch junctions, number of triple branch points, number of branch ends, and cellular perimeter. As in the original paper, features were z score normalized and transformed via principal component analysis with the first 9 principal components (>99% variance retained) used as the input for MORPHIOUS. Following a grid search using 5-fold cross-validation, the final MORPHIOUS

parameters were determined to be Nu: 0.03, minimum distance: 142 μm, gamma: 0.25, and minimum cluster size: 22. Focally activated microglia were detected using a minimum cluster size of 5. For more details on MORPHIOUS, see the original paper.[34]

Cell Profiler quantification

Six sections, 800 μm apart, were immunostained per BALB/c mouse. The BBB permeability is increased within a 1-mm diameter of the ultrasound focus. Therefore, 1 mm diameter single-plane images of each of the four ultrasound spots acquired at 20× were used for quantification of cell transduction using Cell Profiler. This corresponds to a total area of 3.14 mm^2 quantified per brain section, which is larger than the area chosen for quantification previously by us and others,[8,12,67] thus resulting in lower transduction values. Prior to quantification, tiles were stitched using ZEN 2.0.0.0 (blue edition), background was subtracted using ImageJ (FIJI), and images were saved as TIFF files. Cell Profiler 3.1.9 was used to run the pipeline, as outlined in Table S1. A separate dataset consisting of a total of 56 images for GFP$^+$/NeuN$^+$ quantifications and 56 images for GFP$^+$/S100B$^+$ quantifications was first run through the pipeline, and each result was manually verified confirming a high consistency between manual and automatic counting with 2%–4% variability.

SUPPLEMENTAL INFORMATION

Supplemental information can be found online at https://doi.org/10.1016/j.omtm.2021.10.001.

AUTHOR CONTRIBUTIONS

R.H.K., S.H., S.D., K.H., and I.A. designed the experiments. E.M.S. provided viral capsid expertise and the viruses. R.H.K. and S.D. performed the ultrasound experiments. S.H. established staining protocols. R.H.K., M.M., J.S., and C.L.D. processed, immunostained, and analyzed the tissue. R.H.K. and C.L.D. wrote the manuscript draft and created the figures. All authors edited and proofread the manuscript.

DECLARATION OF INTERESTS

The authors declare no competing interests.

REFERENCES

1. Rafii, M.S., Tuszynski, M.H., Thomas, R.G., Barba, D., Brewer, J.B., Rissman, R.A., Siffert, J., and Aisen, P.S.; AAV2-NGF Study Team (2018). Adeno-Associated Viral Vector (Serotype 2)-Nerve Growth Factor for Patients With Alzheimer Disease: A Randomized Clinical Trial. JAMA Neurol. 75, 834–841.

2. Tuszynski, M.H., Yang, J.H., Barba, D., U, H.S., Bakay, R.A.E., Pay, M.M., Masliah, E., Conner, J.M., Kobalka, P., Roy, S., and Nagahara, A.H. (2015). Nerve Growth Factor Gene Therapy: Activation of Neuronal Responses in Alzheimer Disease. JAMA Neurol. 72, 1139–1147.

3. Tuszynski, M.H., Thal, L., Pay, M., Salmon, D.P., U, H.S., Bakay, R., Patel, P., Blesch, A., Vahlsing, H.L., Ho, G., et al. (2005). A phase 1 clinical trial of nerve growth factor gene therapy for Alzheimer disease. Nat. Med. 11, 551–555.

4. Castle, M.J., Baltanás, F.C., Kovacs, I., Nagahara, A.H., Barba, D., and Tuszynski, M.H. (2020). Postmortem analysis in a clinical trial of AAV2-NGF gene therapy for alzheimer's disease identifies a need for improved vector delivery. Hum. Gene Ther. 31, 415–422.

5. Rosenberg, J.B., Kaplitt, M.G., De, B.P., Chen, A., Flagiello, T., Salami, C., Pey, E., Zhao, L., Ricart Arbona, R.J., Monette, S., et al. (2018). AAVrh.10-Mediated APOE2 Central Nervous System Gene Therapy for APOE4-Associated Alzheimer's Disease. Hum. Gene Ther. Clin. Dev. 29, 24–47.

6. Gray, S.J., Matagne, V., Bachaboina, L., Yadav, S., Ojeda, S.R., and Samulski, R.J. (2011). Preclinical differences of intravascular AAV9 delivery to neurons and glia: a comparative study of adult mice and nonhuman primates. Mol. Ther. 19, 1058–1069.

7. Ertl, H.C.J., and High, K.A. (2017). Impact of AAV Capsid-Specific T-Cell Responses on Design and Outcome of Clinical Gene Transfer Trials with Recombinant Adeno-Associated Viral Vectors: An Evolving Controversy. Hum. Gene Ther. 28, 328–337.

8. Thévenot, E., Jordão, J.F., O'Reilly, M.A., Markham, K., Weng, Y.-Q., Foust, K.D., Kaspar, B.K., Hynynen, K., and Aubert, I. (2012). Targeted delivery of self-complementary adeno-associated virus serotype 9 to the brain, using magnetic resonance imaging-guided focused ultrasound. Hum. Gene Ther. 23, 1144–1155.

9. Deverman, B.E., Pravdo, P.L., Simpson, B.P., Kumar, S.R., Chan, K.Y., Banerjee, A., Wu, W.-L., Yang, B., Huber, N., Pasca, S.P., and Gradinaru, V. (2016). Cre-dependent selection yields AAV variants for widespread gene transfer to the adult brain. Nat. Biotechnol. 34, 204–209.

10. Hynynen, K., McDannold, N., Vykhodtseva, N., and Jolesz, F.A. (2001). Noninvasive MR imaging-guided focal opening of the blood-brain barrier in rabbits. Radiology 220, 640–646.

11. Lipsman, N., Meng, Y., Bethune, A.J., Huang, Y., Lam, B., Masellis, M., Herrmann, N., Heyn, C., Aubert, I., Boutet, A., et al. (2018). Blood-brain barrier opening in Alzheimer's disease using MR-guided focused ultrasound. Nat. Commun. 9, 2336.

12. Hsu, P.-H., Wei, K.-C., Huang, C.-Y., Wen, C.-J., Yen, T.-C., Liu, C.-L., Lin, Y.-T., Chen, J.-C., Shen, C.-R., and Liu, H.-L. (2013). Noninvasive and targeted gene delivery into the brain using microbubble-facilitated focused ultrasound. PLoS ONE 8, e57682.

13. Weber-Adrian, D., Thévenot, E., O'Reilly, M.A., Oakden, W., Akens, M.K., Ellens, N., Markham-Coultes, K., Burgess, A., Finkelstein, J., Yee, A.J.M., et al. (2015). Gene delivery to the spinal cord using MRI-guided focused ultrasound. Gene Ther. 22, 568–577.

14. Wang, S., Olumolade, O.O., Sun, T., Samiotaki, G., and Konofagou, E.E. (2015). Noninvasive, neuron-specific gene therapy can be facilitated by focused ultrasound and recombinant adeno-associated virus. Gene Ther. 22, 104–110.

15. Weber-Adrian, D., Kofoed, R.H., Chan, J.W.Y., Silburt, J., Noroozian, Z., Kügler, S., Hynynen, K., and Aubert, I. (2019). Strategy to enhance transgene expression in proximity of amyloid plaques in a mouse model of Alzheimer's disease. Theranostics 9, 8127–8137.

16. Hordeaux, J., Yuan, Y., Clark, P.M., Wang, Q., Martino, R.A., Sims, J.J., Bell, P., Raymond, A., Stanford, W.L., and Wilson, J.M. (2019). The GPI-Linked Protein LY6A Drives AAV-PHP.B Transport across the Blood-Brain Barrier. Mol. Ther. 27, 912–921.

17. Huang, Q., Chan, K.Y., Tobey, I.G., Chan, Y.A., Poterba, T., Boutros, C.L., Balazs, A.B., Daneman, R., Bloom, J.M., Seed, C., and Deverman, B.E. (2019). Delivering genes across the blood-brain barrier: LY6A, a novel cellular receptor for AAV-PHP.B capsids. PLoS ONE 14, e0225206.

18. Batista, A.R., King, O.D., Reardon, C.P., Davis, C., Shankaracharya, Philip, V., Gray-Edwards, H., Aronin, N., Lutz, C., Landers, J., and Sena-Esteves, M. (2020). Ly6a Differential Expression in Blood-Brain Barrier Is Responsible for Strain Specific Central Nervous System Transduction Profile of AAV-PHP.B. Hum. Gene Ther. 31, 90–102.

19. Matsuzaki, Y., Konno, A., Mochizuki, R., Shinohara, Y., Nitta, K., Okada, Y., and Hirai, H. (2018). Intravenous administration of the adeno-associated virus-PHP.B capsid fails to upregulate transduction efficiency in the marmoset brain. Neurosci. Lett. 665, 182–188.

20. Hordeaux, J., Wang, Q., Katz, N., Buza, E.L., Bell, P., and Wilson, J.M. (2018). The neurotropic properties of AAV-PHP.B are limited to C57BL/6J mice. Mol. Ther. 26, 664–668.

21. Toledo, J.B., Arnold, S.E., Raible, K., Brettschneider, J., Xie, S.X., Grossman, M., Monsell, S.E., Kukull, W.A., and Trojanowski, J.Q. (2013). Contribution of cerebrovascular disease in autopsy confirmed neurodegenerative disease cases in the National Alzheimer's Coordinating Centre. Brain 136, 2697–2706.

22. Spangenberg, E.E., and Green, K.N. (2017). Inflammation in Alzheimer's disease: Lessons learned from microglia-depletion models. Brain Behav. Immun. 61, 1–11.

23. Chishti, M.A., Yang, D.-S., Janus, C., Phinney, A.L., Horne, P., Pearson, J., Strome, R., Zuker, N., Loukides, J., French, J., et al. (2001). Early-onset amyloid deposition and cognitive deficits in transgenic mice expressing a double mutant form of amyloid precursor protein 695. J. Biol. Chem. 276, 21562–21570.

24. Selkoe, D.J., and Hardy, J. (2016). The amyloid hypothesis of Alzheimer's disease at 25 years. EMBO Mol. Med. 8, 595–608.

25. de Leeuw, C.N., Korecki, A.J., Berry, G.E., Hickmott, J.W., Lam, S.L., Lengyell, T.C., Bonaguro, R.J., Borretta, L.J., Chopra, V., Chou, A.Y., et al. (2016). rAAV-compatible MiniPromoters for restricted expression in the brain and eye. Mol. Brain 9, 52.

26. Dubey, S., Heinen, S., Krantic, S., McLaurin, J., Branch, D.R., Hynynen, K., and Aubert, I. (2020). Clinically approved IVIg delivered to the hippocampus with focused ultrasound promotes neurogenesis in a model of Alzheimer's disease. Proc. Natl. Acad. Sci. USA 117, 32691–32700.

27. Xhima, K., Markham-Coultes, K., Nedev, H., Heinen, S., Saragovi, H.U., Hynynen, K., and Aubert, I. (2020). Focused ultrasound delivery of a selective TrkA agonist rescues cholinergic function in a mouse model of Alzheimer's disease. Sci. Adv. 6, eaax6646.

28. Samaranch, L., Sebastian, W.S., Kells, A.P., Salegio, E.A., Heller, G., Bringas, J.R., Pivirotto, P., DeArmond, S., Forsayeth, J., and Bankiewicz, K.S. (2014). AAV9-mediated expression of a non-self protein in nonhuman primate central nervous system triggers widespread neuroinflammation driven by antigen-presenting cell transduction. Mol. Ther. 22, 329–337.

29. Ciesielska, A., Hadaczek, P., Mittermeyer, G., Zhou, S., Wright, J.F., Bankiewicz, K.S., and Forsayeth, J. (2013). Cerebral infusion of AAV9 vector-encoding non-self proteins can elicit cell-mediated immune responses. Mol. Ther. 21, 158–166.

30. Hadaczek, P., Forsayeth, J., Mirek, H., Munson, K., Bringas, J., Pivirotto, P., McBride, J.L., Davidson, B.L., and Bankiewicz, K.S. (2009). Transduction of nonhuman primate

brain with adeno-associated virus serotype 1: vector trafficking and immune response. Hum. Gene Ther. 20, 225–237.

31. Amado, D.A., Rieders, J.M., Diatta, F., Hernandez-Con, P., Singer, A., Mak, J.T., Zhang, J., Lancaster, E., Davidson, B.L., and Chen-Plotkin, A.S. (2019). AAV-Mediated Progranulin Delivery to a Mouse Model of Progranulin Deficiency Causes T Cell-Mediated Toxicity. Mol. Ther. 27, 465–478.

32. Zaiss, A.K., Cotter, M.J., White, L.R., Clark, S.A., Wong, N.C.W., Holers, V.M., Bartlett, J.S., and Muruve, D.A. (2008). Complement is an essential component of the immune response to adeno-associated virus vectors. J. Virol. 82, 2727–2740.

33. Vandamme, C., Adjali, O., and Mingozzi, F. (2017). Unraveling the complex story of immune responses to AAV vectors trial after trial. Hum. Gene Ther. 28, 1061–1074.

34. Silburt, J., and Aubert, I. (2020). Not peer review manuscript: MORPHIOUS: A Machine Learning Workflow to Naively Detect the Activation of Microglia and Astrocytes. bioRxiv. https://doi.org/10.1101/2020.08.17.251843.

35. Toapanta, F.R., and Ross, T.M. (2006). Complement-mediated activation of the adaptive immune responses: role of C3d in linking the innate and adaptive immunity. Immunol. Res. 36, 197–210.

36. Loughner, C.L., Bruford, E.A., McAndrews, M.S., Delp, E.E., Swamynathan, S., and Swamynathan, S.K. (2016). Organization, evolution and functions of the human and mouse Ly6/uPAR family genes. Hum. Genomics 10, 10.

37. Soylemezoglu, F., Onder, S., Tezel, G.G., and Berker, M. (2003). Neuronal nuclear antigen (NeuN): a new tool in the diagnosis of central neurocytoma. Pathol. Res. Pract. 199, 463–468.

38. Duan, W., Zhang, Y.P., Hou, Z., Huang, C., Zhu, H., Zhang, C.Q., and Yin, Q. (2016). Novel Insights into NeuN: from Neuronal Marker to Splicing Regulator. Mol. Neurobiol. 53, 1637–1647.

39. Steiner, J., Bernstein, H.G., Bielau, H., Berndt, A., Brisch, R., Mawrin, C., Keilhoff, G., and Bogerts, B. (2007). Evidence for a wide extra-astrocytic distribution of S100B in human brain. BMC Neurosci. 8, 2.

40. Zhang, Z., Ma, Z., Zou, W., Guo, H., Liu, M., Ma, Y., and Zhang, L. (2019). The Appropriate Marker for Astrocytes: Comparing the Distribution and Expression of Three Astrocytic Markers in Different Mouse Cerebral Regions. BioMed Res. Int. 2019, 9605265.

41. Foiret, J., Zhang, H., Fite, B.Z., Ilovitsh, T., Mahakian, L.M., Tam, S., Beitnere, U., Pyles, B., Segal, D.J., and Ferrara, K.W. (2017). Blood-brain barrier disruption for the delivery of non-infectious viral vectors and proteins, preliminary study. IEEE Int. Ultrason. Symp. IUS, 1–4.

42. Rossi, A., Dupaty, L., Aillot, L., Zhang, L., Gallien, C., Hallek, M., Odenthal, M., Adriouch, S., Salvetti, A., and Büning, H. (2019). Vector uncoating limits adeno-associated viral vector-mediated transduction of human dendritic cells and vector immunogenicity. Sci. Rep. 9, 3631.

43. Verdera, H.C., Kuranda, K., and Mingozzi, F. (2020). AAV Vector Immunogenicity in Humans: A Long Journey to Successful Gene Transfer. Mol. Ther. 28, 723–746.

44. Mendell, J.R., Al-Zaidy, S., Shell, R., Arnold, W.D., Rodino-Klapac, L.R., Prior, T.W., Lowes, L., Alfano, L., Berry, K., Church, K., et al. (2017). Single-Dose Gene-Replacement Therapy for Spinal Muscular Atrophy. N. Engl. J. Med. 377, 1713–1722.

45. Lim, J.A., Yi, H., Gao, F., Raben, N., Kishnani, P.S., and Sun, B. (2019). Intravenous Injection of an AAV-PHP.B Vector Encoding Human Acid α-Glucosidase Rescues Both Muscle and CNS Defects in Murine Pompe Disease. Mol. Ther. Methods Clin. Dev. 12, 233–245.

46. Jordão, J.F., Thévenot, E., Markham-Coultes, K., Scarcelli, T., Weng, Y.Q., Xhima, K., O'Reilly, M., Huang, Y., McLaurin, J., Hynynen, K., and Aubert, I. (2013). Amyloid-β plaque reduction, endogenous antibody delivery and glial activation by brain-targeted, transcranial focused ultrasound. Exp. Neurol. 248, 16–29.

47. Gao, G., Wang, Q., Calcedo, R., Mays, L., Bell, P., Wang, L., Vandenberghe, L.H., Grant, R., Sanmiguel, J., Furth, E.E., and Wilson, J.M. (2009). Adeno-associated virus-mediated gene transfer to nonhuman primate liver can elicit destructive transgene-specific T cell responses. Hum. Gene Ther. 20, 930–942.

48. Forsayeth, J., and Bankiewicz, K.S. (2015). Transduction of antigen-presenting cells in the brain by AAV9 warrants caution in preclinical studies. Mol. Ther. 23, 612.

49. Chan, K.Y., Jang, M.J., Yoo, B.B., Greenbaum, A., Ravi, N., Wu, W.L., Sánchez-Guardado, L., Lois, C., Mazmanian, S.K., Deverman, B.E., and Gradinaru, V.

(2017). Engineered AAVs for efficient noninvasive gene delivery to the central and peripheral nervous systems. Nat. Neurosci. 20, 1172–1179.

50. Biswas, M., Kumar, S.R.P., Terhorst, C., and Herzog, R.W. (2018). Gene therapy with regulatory T cells: A beneficial alliance. Front. Immunol. 9, 554.

51. Colella, P., Sellier, P., Costa Verdera, H., Puzzo, F., van Wittenberghe, L., Guerchet, N., Daniele, N., Gjata, B., Marmier, S., Charles, S., et al. (2018). AAV Gene Transfer with Tandem Promoter Design Prevents Anti-transgene Immunity and Provides Persistent Efficacy in Neonate Pompe Mice. Mol. Ther. Methods Clin. Dev. 12, 85–101.

52. Wang, S., Leem, J.S., Podvin, S., Hook, V., Kleschevnikov, N., Savchenko, P., Dhanani, M., Zhou, K., Kelly, I.C., Zhang, T., et al. (2021). Synapsin-caveolin-1 gene therapy preserves neuronal and synaptic morphology and prevents neurodegeneration in a mouse model of AD. Mol. Ther. Methods Clin. Dev. 21, 434–450.

53. Jackson, K.L., Dayton, R.D., Deverman, B.E., and Klein, R.L. (2016). Better Targeting, Better Efficiency for Wide-Scale Neuronal Transduction with the Synapsin Promoter and AAV-PHP.B. Front. Mol. Neurosci. 9, 116.

54. Galvan, A., Petkau, T.L., Hill, A.M., Korecki, A.J., Lu, G., Choi, D., Rahman, K., Simpson, E., Leavitt, B.R., and Smith, Y. (2021). Intracerebroventricular Administration of AAV9-PHP.B SYN1-EmGFP Induces Widespread Transgene Expression in the Mouse and Monkey CNS. Hum. Gene Ther. 32, 599–615.

55. Weber-Adrian, D., Kofoed, R.H., Silburt, J., Noroozian, Z., Shah, K., Burgess, A., Rideout, S., Kügler, S., Hynynen, K., and Aubert, I. (2021). Systemic AAV6-synapsin-GFP administration results in lower liver biodistribution, compared to AAV1&2 and AAV9, with neuronal expression following ultrasound-mediated brain delivery. Sci. Rep. 11, 1934.

56. Simpson, E.M., Korecki, A.J., Fornes, O., McGill, T.J., Cueva-Vargas, J.L., Agostinone, J., Farkas, R.A., Hickmott, J.W., Lam, S.L., Mathelier, A., et al. (2019). New MiniPromoter Ple345 (NEFL) Drives Strong and Specific Expression in Retinal Ganglion Cells of Mouse and Primate Retina. Hum. Gene Ther. 30, 257–272.

57. Korecki, A.J., Cueva-Vargas, J.L., Fornes, O., Agostinone, J., Farkas, R.A., Hickmott, J.W., Lam, S.L., Mathelier, A., Zhou, M., Wasserman, W.W., et al. (2021). Human MiniPromoters for ocular-rAAV expression in ON bipolar, cone, corneal, endothelial, Müller glial, and PAX6 cells. Gene Ther. 28, 351–372.

58. Hickmott, J.W., Chen, C.Y., Arenillas, D.J., Korecki, A.J., Lam, S.L., Molday, L.L., Bonaguro, R.J., Zhou, M., Chou, A.Y., Mathelier, A., et al. (2016). PAX6 MiniPromoters drive restricted expression from rAAV in the adult mouse retina. Mol. Ther. Methods Clin. Dev. 3, 16051.

59. Teerawanichpan, P., Hoffman, T., Ashe, P., Datla, R., and Selvaraj, G. (2007). Investigations of combinations of mutations in the jellyfish green fluorescent protein (GFP) that afford brighter fluorescence, and use of a version (VisGreen) in plant, bacterial, and animal cells. Biochim. Biophys. Acta 1770, 1360–1368.

60. Zanta-Boussif, M.A., Charrier, S., Brice-Ouzet, A., Martin, S., Opolon, P., Thrasher, A.J., Hope, T.J., and Galy, A. (2009). Validation of a mutated PRE sequence allowing high and sustained transgene expression while abrogating WHV-X protein synthesis: application to the gene therapy of WAS. Gene Ther. 16, 605–619.

61. Zufferey, R., Donello, J.E., Trono, D., and Hope, T.J. (1999). Woodchuck hepatitis virus posttranscriptional regulatory element enhances expression of transgenes delivered by retroviral vectors. J. Virol. 73, 2886–2892.

62. Foust, K.D., Nurre, E., Montgomery, C.L., Hernandez, A., Chan, C.M., and Kaspar, B.K. (2009). Intravascular AAV9 preferentially targets neonatal neurons and adult astrocytes. Nat. Biotechnol. 27, 59–65.

63. Noroozian, Z., Xhima, K., Huang, Y., Kaspar, B.K., Kügler, S., Hynynen, K., and Aubert, I. (2019). MRI-guided focused ultrasound for targeted delivery of rAAV to the brain. Methods Mol. Biol. 1950, 177–197.

64. Touahri, Y., Dixit, R., Kofoed, R.H., Miloska, K., Park, E., Raeisossadati, R., Markham-Coultes, K., David, L.A., Rijal, H., Zhao, J., et al. (2020). Focused ultrasound as a novel strategy for noninvasive gene delivery to retinal Müller glia. Theranostics 10, 2982–2999.

65. O'Reilly, M.A., and Hynynen, K. (2012). Blood-brain barrier: real-time feedback-controlled focused ultrasound disruption by using an acoustic emissions-based controller. Radiology 263, 96–106.

66. Legland, D., Arganda-Carreras, I., and Andrey, P. (2016). MorphoLibJ: integrated library and plugins for mathematical morphology with ImageJ. Bioinformatics 32, 3532–3534.

67. Stavarache, M.A., Petersen, N., Jurgens, E.M., Milstein, E.R., Rosenfeld, Z.B., Ballon, D.J., and Kaplitt, M.G. (2018). Safe and stable noninvasive focal gene delivery to the mammalian brain following focused ultrasound. J. Neurosurg. 130, 989–998.